Estimation of near surface shear wave velocity using CMP cross-correlation of surface waves (CCSW)

Roohollah Askari, Robert J. Ferguson and Kristof DeMeersman

ABSTRACT

One of the challenges of converted wave processing is to estimate a good near surface shear wave velocity model for static corrections. To this end, we have enlarged upon the idea of CMP Cross-Correlation of Surface Waves to increase lateral resolution. Our approach is fast and we believe it is more robust in the presence of variable source wavelet and noise. We cross-correlate each trace of a shot record is with a reference trace that is selected from within the shot gather based on high signal to noise ration. This step removes source effect, and converts traces to zero-phase. New midpoints that relate to the correlated traces are then calculated. We calculate the phase velocity for each CMP gather, and finally, we convert the resulting dispersion curve to a vertical shear wave velocity by an inverse procedure. Putting together all the vertical shear wave velocity profiles of all the CMP gathers, 2D images of shear wave velocity are obtained for the data set. In this study, we invert for 2D shear wave profiles for two receiver lines with different geophone spacing. We have used the models to compute converted wave receiver statics, and our results illustrate the potential use of this method for computing converted wave receiver static corrections.

INTRODUCTION

Spectral Analysis of Surface Waves (SASW) (Nazarian et al., 1983) is a conventional method for the determination of 1D shear wave velocity for the near surface. The ground roll fundamental mode is analyzed by configuring and reconfiguring a pair of receivers and shots respectively. Park et al. (1999a) introduce the Multi-channel Analysis of Surface Waves (MASW) method where a dispersion curve for a multi-channel data set is estimated by transforming (e.g. the phase shift method (Park et al., 1998)) the data from the time-offset domain to the frequency-slowness (or velocity) domain. Generally speaking, in a MASW survey, the calculation of dispersion curves is faster and more accurate than those for SASW because we can isolate and distinguish other unwanted coherent event such as first arrivals, higher modes and air waves. Furthermore, MASW is less affected by ambient noise and provides a better signal to noise ratio (Hayashi and Suzuki, 2004). Therefore, MASW results in a better dispersion curve estimation, but it does at the cost of lateral resolution because of the long receiver array that must be used (Park et al., 1999b). Smaller arrays should be used when we need a better lateral resolution, but this reduces the resolution of the dispersion curve. Therefore, there is a tradeoff between the estimation of the dispersion curve and lateral resolution. In practice, it is critical to compensate for this tradeoff. Especially in converted wave surveys, rapid spatial velocity variations in the weathering layer need to be resolved in order to compute an appropriate velocity model for the static corrections. This requires both excellent quality phase velocity information as well as high spatial resolution.

In this study, we have enlarged upon the idea of CMP Cross-Correlation of Surface Waves (CCSW Hayashi and Suzuki, 2004) to increase lateral resolution. In the Hayashi and Suzuki's methodology, all traces within a common mid-point (CMP) are correlated with each other, traces with the same offset which belong the same CMP are stacked, and a dispersion curve is computed. Though this method provides a good lateral resolution and dispersion curve simultaneously, the process is computationally expensive. Therefore in our approach, to reduce cost and to improve noise tolerance, we cross-correlate each trace of a shot record is with a reference trace that is selected from within the shot gather based on high signal to noise ration. This step removes the source effect, and converts traces to zero-phase. New midpoints that relate to the correlated traces are then calculated. We calculate the phase velocity for each CMP gather, and finally, the dispersion curve is converted to a vertical shear wave velocity by an inverse procedure. Putting together all the vertical shear wave velocity profiles of all the CMP gathers, a 2D image of shear wave velocity is obtained for the data set.

In this study, we use two different data sets with different acquisition parameters. The first data set is a receiver line with 10m geophone spacing that was extracted from a 3D seismic survey. The S velocity model obtained from the method shows a well coherent match to the P velocity model obtained from turning wave tomography. This shows the promising potential of the method for near surface S velocity imaging. We have used the model to compute converted wave receiver statics. Though our results show a good match with the static corrections obtained from a trim static, in general, low velocity abnormalities are not well detected. This is mostly due to weak acquisition. These low velocity abnormalities are caused by buried channel in the region with 5-10m diameters. Therefore, finer geophone spacing should have been used in order to detect those channels. In the second data set, we used a line from a multi component survey with 2m geophone spacing. The detailed map of the phase velocity shows the potential of the method for the static corrections of converted waves.

THEORY

Assuming that a geometrical spreading correction has been applied to surface wave data, if $h_1(t)$ is the signal recorded at station 1, then $h_2(t)$, the recorded signal at station 2, can be expressed by (Askari and Ferguson, 2011)

$$H_2(f) = e^{-\lambda(f)d} e^{-j2\pi k(f)x_1} H_1(f), \quad (1)$$

where $\lambda(f)$ is an attenuation function, $k(f)$ is a spatial wave number that controls wave propagation from station 1 to station 2, and x_1 is the distance between two stations. For any station, such as station 3, equation 1 is consistent. Therefore for any specific frequency, the spatial wave number can be obtained by

$$K(f) = -\frac{\varphi_{3(f)} - \varphi_2(f)}{2\pi\Delta x} = -\frac{\Delta\varphi(f)}{2\pi\Delta x}, \quad (2)$$

where φ_2 and φ_3 are the absolute phase spectra of stations 2 and 3 respectively and Δx is the distance between two stations.

If we cross-correlate the first trace with the traces of stations 2 and 3, for station 2 the cross-correlated trace is expressed in the Fourier domain as

$$C(H_1(f), H_2(f)) = e^{-\lambda(f)d} e^{-j2\pi k(f) x_1} H_1(f) H_1^*(f), \quad (3)$$

where H_1^* is the complex conjugate of H_1. With respect to equation 3, which can be written for other traces such as h_3, the spatial wave number can be estimated by

$$K(f) = -\frac{\emptyset_{3(f)} - \emptyset_2(f)}{2\pi\Delta x} = -\frac{\Delta\emptyset(f)}{2\pi\Delta x}, \quad (4)$$

where $\emptyset_2$ and $\emptyset_3$ are the absolute phase spectra of the cross-correlated traces of stations 1 and 2 and stations 1 and 3 respectively. Following calculation of the wavenumber K, the phase velocity is obtained as

$$v_p = \frac{f}{k(f)}. \quad (5)$$

We use the approach expressed in equation 3 for the calculation of the phase velocity. Because the source effect (initial phase value) is removed, therefore, the data can be sorted CMP gathers. Consequently, we calculate the phase velocity of traces in one CMP combined from different shots to localize our analysis spatially. In this study, we use the phase shift method (Park et al. 1998) for the calculation of the phase velocity. The method is based on the estimation of the phase differences (shifts) of different traces for a range of frequencies. The method is able to estimate the phase velocity of multi-modal ground-roll (Askari et al., 2011).

FIRST DATA SET

We use a 2D receiver line that was extracted from a 3D-3C accelerometer Alberta oil sands survey. The line is composed of 78 shots and 10206 traces. Among these traces, 7627 traces are selected based on their high signal to noise ratio. The geophone interval is 10m and the sampling rate is 1ms. Each trace is cross-correlated with a near-offset reference trace in order to remove the source phase. The data are binned using a CMP bin size of 10m, which is twice the natural bin size. We did this to increase fold so as to allow for a more stable phase velocity analysis. Figure 1 shows traces in a bin. The traces are zero phase and they are regularly spaces. We calculate the phase velocity using the method of Phase Shift (Park et al., 1998). Figure 2 shows the phase velocity that is calculated for the data in Figure 1. Only the fundamental mode is detectable because the geophone interval is too large for higher modes. Higher modes are usually composed of higher frequencies. Therefore, they are highly scattered for large travel distances and consequently their phase velocity cannot be detected when geophone intervals are too large. Analyzing all the data in the bins, we have finally 83 bins in which the phase velocity is well detectable. Figure 3 shows a 2D image of the phase velocity for all the bins. With respect to the dependency of depth to frequency and phase velocity, at low frequencies (deeper layers), we can see higher phase velocity. On the other hand, at low frequencies (shallower layers), the phase velocity is smaller. These observations are consistent with other studies (e.g. Evison et al., 1959; Stokoe et al., 1988; Keilis- Borok, 1989; Lay and Wallace, 1995; Xia et al., 1999). The 2D image of the phase velocity shows consistency and coherency with what we expect from a real model.

DATA INVERSION

We can forward model dispersion curves for any geological 1D model using Knopoff's method (Schwab and Knopoff, 1972). The Rayleigh-wave phase velocity, c_j, is determined by a nonlinear equation 'F'in an implicit form:

$$F(\ f\ ,c_f\ ,\mathbf{v_s}\ ,\mathbf{v_p},\ \rho,\ \mathbf{h}) = 0 \quad (j = 1, 2, \ldots ,m), \tag{6}$$

where f is the frequency, $\mathbf{v_s}$ and $\mathbf{v_p}$ denote the S and P wave velocities respectively, **h** is the thicknesses of layers, ρ is the densities of the layers and, cf is the calculated phase velocity. Using the above equation, we try to optimize a model using the method of Steepest Descent (Zeidouni, 2011).

We calculate the dispersion function's derivatives for a synthetic geological model (Table 1). We increase the S velocity, P velocity, and the density of the fifth layer about %20 to calculate the derivatives. Figure 4 shows the calculated derivatives for the S velocity, P velocity, and density respectively. The phase velocity is more sensitive to the variation of the S velocity. Therefore, we assume constant P velocity and density (Xia et al., 1999). These values are determined from turning wave tomography (Figure 5) and a density log respectively. The density is chosen to be 2000 kg/m^3.

$$\mathrm{Cov}(m) = s^2([J^T][J])^{-1}, \tag{7}$$

where J is a Jacobin matrix and s is the standard deviation of data which is obtained by

$$s = \sqrt{\frac{\|c_{obs} - c_{est}\|^2}{(n-m)}}, \tag{8}$$

where c_{obs} is the observed phase velocity, c_{est} is the estimated phase velocity, n is the number of data parameters and m is the number of model parameters. Figure 6 shows the standard deviation of the model parameters and we conclude that the data have little uncertainty (less than 200 m/s) for the depth for the surface to about 60m. Therefore we trust the inversion results from the surface to 60m. Figure 7 shows the S velocity model obtained from the inversion, and we can see that there is comparable well match to the P velocity model (Figure 8).

STATIC CORRECTION

We then estimate static correction based on the obtained S velocity model for converted waves. Figure 8 shows a record from horizontal geophones containing PS reflectors without static correction. We have applied CCSW static correction to the data (Figure 9). The velocity model cannot flatten the reflectors with significant short wave-length statics issues (red circles). We assume there are two local low velocity abnormalities indicated by the red circles that cause bulk time shifts. The abnormalities imply that the method cannot provide us with enough lateral resolution when there is a local low velocity zone. Figure 10 shows the shot record with static correction which was obtained from a non-physical trim static method also known as the horizon based approach. Here, a horizon from the same geological interface is picked on both the PP and PS receiver stack. An S-wave receiver static can be obtained by differencing the PS horizon with the PP horizon that is stretched to PS time. Figure 11 shows static

corrections obtained from horizontal based and CCSW methods respectively. Figure 11 shows that there are three velocity abnormalities at A, B and C that CCSW cannot detect.

We consider a number of explanations for our results. The first is a fundamental mode limitation in the resolution of our analysis method. Other authors have proposed the use of higher modes to improve vertical resolution (Luo et al., 2007). It can be expected that incorporating the fundamental mode with higher modes will result in a better lateral resolution as well. Other more important factors are variations in survey design and local geology. We think these factors are the main cause of the poor static results.

In the area of study, there are some buried channels with 5-10m diameters reminded from glassier. These channels sometimes create local low velocity abnormalities that can be only observed in few geophones. In order to detect these abnormalities, finer geophone spacing should be used. In this data set, geophone spacing is 10m which is not suitable for detecting buried 5-10m diameter channels. We use another data set with 2m geophone spacing to see how lateral resolution will improve when finer geophone spacing is used.

SECOND DATA SET

The second data set used in this study is acquired from a site near Priddis, Alberta, about 30 km southwest of the city of Calgary. The site of the survey is located at the eastern edge of the Rocky Mountain foothills. The geophones are 3C SM7 with 2m geophone spacing and 1ms time sampling. Vibroseis is used in each 4m. The sweep frequency varies from 10Hz to 120Hz and duration time is 10s. We repeat the same process applied to the first data set. However, due to the ranges of frequencies that we observe in the Priddis data (11-30Hz), we realize that the maximum depth that we can obtain more reasonable results from inversion is 20m. Therefore, we select those geophones for processing which are limited in the offset ranges from 30-100m in order to have optimum parameters for S velocity inversion (Park et. al., 2002). We merge each five CMP gathers in one bin in order to have good folds. The fundamental mode is only considered for inversion because it is more strong and obvious in most bins. Preliminarily, we consider the vertical component for the phase velocity estimation. However, if in some specific bins in which a clear dispersion curve is not well detectable on the vertical component, we consider radial component as well.

If the dispersion curve on the radial component is better observable than that on the vertical component, we choose it as the observed phase velocity for that bin and ignore vertical component. But, if both components do not show clear dispersion curves, we estimate dispersion curves on the both components separately; calculate an average of them; and consider it as the observed phase velocity. Figures 12a and 12b show the vertical and radial components in a bin respectively. Figures 12c and 12d show the observed phase velocity on the vertical and radial components respectively. We can observe two distinct curves in Figure 12d which can be referred to the fundamental mode (the left curve) and the first higher mode (the right curve). However, the first higher mode is only detectable on the vertical component (Figure 12c). Since, only fundamental mode is interesting for us in this study, we estimate it on the redial component for this bin. This demonstrates that we should consider both components when we process data.

We obtained the phase velocity for 60 bins. Figure 13 shows the observed phase velocity of all the bins. Comparing Figure 13 with Figure 3, it can be concluded that the phase velocity in Figure 13 is not as smooth as the phase velocity in Figure 3 because geophone spacing is finer in the Priddis data and thus we record higher frequencies. Therefore, Figure 13 implies more details about subsurface. It is expected that inverted S velocity from Figure 13, provides us with more details about near surface.

For data inversion we choose density 2300 kg/m^3 based on several logs that we have in the studied area. We did not have any P velocity model for the Priddis data. Therefore, we assign an estimation of P velocity based on the S velocity and the Poisson ratio

$$V_p = V_s\left(\frac{1-\sigma}{0.5-\sigma}\right)^{\frac{1}{2}}, \tag{9}$$

where σ denotes the Poisson ratio. We repeat the inversion process for ranges of Poisson ratios from 0.4 to 0.496 which are commonly observed for the near surface (e.g. Ivanov et al., 2000). For each bin, we select the Poisson ratio which gives the best fit (less RMS error) and assign it to that bin. Figure 14 show the S velocity model obtained from Figure 13. Some geological structures at the depths 7.5m and 18m are noticeable. It implies the high potential of CCSW for near surface imaging when optimum acquisition parameters are used. Figure 14 show the estimated Poisson ratios.

CONCLUSION

We introduce a new approach of the CMP Cross-Correlation of Surface Wave in order to obtain a better lateral resolution for near surface S velocity imaging. The idea takes advantages of SASW and MASW methods, and also is faster than the conventional CCSW (Hayashi and Suzuki, 2004) and more robust in the presence of variable source wavelet and noise. The S velocity model obtained from the method shows a good coherency to the P velocity model. This shows the potential use of the method for a better lateral resolution of S velocity imaging.

The consistency of the 2D S velocity image of CCSW with the 2D P velocity image of tomography in the first data set, the detailed S velocity map of the Priddis data, and also other studies done in the literature (e.g. Xia et al, 2002a; Xia et al, 2002b; Strobbia et al. 2011) demonstrate the high potential of the method to be utilized in seismic exploration. Surface waves provide information on the earth's layers nearest to the earth's surface. Our ability to successfully extract information from converted waves and S-waves is dramatically hampered by our lack of understanding of the near-surface S-wave velocity structure. This is exactly why the surface wave methods should be taken into account by the oil and gas industry. However, if we want to obtain more reliable results from surface wave, we have to optimize acquisition parameters. In addition, in order to promote results, we should consider the limitations of surface-wave methods such as the modal superposition which can cause error in the estimation of the phase velocity.

ACKNOWLEDGEMENTS

The authors wish to express their gratitude to CREWES and its sponsors for their generous support. We express our appreciation to Dr. Robert Herrmann for providing Computer Programs in Seismology, Dr. Helen Isaac for processing the Priddis data, and, Dr. Sergio Grion and Dr. Rolf Maier for useful discussions and reviewing this paper. We thank Petrobank for providing the first data set and CGGVeritas for facilitating a part of this research.

REFERENCES

Askari, R., R. J. Ferguson, and K. DeMeersman, 2012, Estimation of phase and group velocities for multi-modal ground roll using the 'phase shift' and 'slant stack generalized S transform based' methods: CREWES Research Report, **23**, paper 4.

Evison, F. F., R. H. Orr, and C. E. Ingham, 1959, Thickness of the earth's crust in Antarctica: Nature, **183**, 306–308.

Haney, M., and Douma, H., 2012, Rayleigh wave tomography at Coronation Field, Canada: The topography effect: The Leading Edge, **31**, 54-61.

Hayashi, K., and H. Suzuki, 2004, CMP cross-correlation analysis of multi-channel surface-wave data: Exploration Geophysics, **35**, 7–13.

Keilis-Borok, V. I., 1989, Seismic surface waves in laterally inhomogeneous earth: Kluwer Academic Publishers.

Lay, T., and T. C. Wallace, 1995, Modern global seismology: Academic Press.

Luo, Y., J. Xia, R. Miller, Y. Xu, J. Liu, and Q. Liu, 2008, Rayleigh-wave dispersive energy imaging using a high-resolution linear Radon transform: Pure and Applied Geophysics, **165**, 903–922.

Ivanov, J., C. B. Park, R. Miller, and J. Xia, 2000, Mapping Poisson's ratio of unconsolidated materials from a joint analysis of surface-wave and refraction events: Proceedings of the Symposium on the Application of Geophysics to Engineering and Environmental Problems (SAGEEP 2000), Arlington, VA, February 20–24, 11–20

Nazarian, S., K. H. Stokoe, and W. R. Hudson, 1983, Use of spectral analysis of surface waves method for determination of moduli and thickness of pavement system: Transportation Research Record, **930**, 38–45.

Park, C. B., R. D. Miller, and J. Xia, 1998, Imaging dispersion curves of surface waves on multi-channel record: 68th Annual International Meeting, SEG, Expanded Abstracts, 1377–1380.

Park, C. B., R. D. Miller, and J. Xia, 1999a, Multichannel analysis of surface waves: Geophysics, **64**, 800–808.

Park, C. B., R. D. Miller, and J. Xia, 1999b, Multimodal analysis of high frequency surface waves: Proceedings of the Symposium on the Application of Geophysics to Engineering and Environmental Problems (SAGEEP), 115–121.

Park, C. B., Miller, R. D., and Miura, H., 2002, Optimum field parameters of an MASW survey: SEG-J, Tokyo, 22–23.

Schwab, F. A., and L. Knopoff, 1972, Fast surface wave and free mode computations, in B. A. Bolt, ed., Methods in computational physics: Academic Press, 87–180.

Strobbia, C., Laake, A., Vermeer, P., and Glushchenko A., 2011, Surface waves: use them then lose them. Surface-wave analysis, inversion and attenuation in land reflection seismic surveying: Near Surface Geophysics, **9**, 503-514

Stokoe, K. H., II, S. Nazarian, G. J. Rix, I. Sanchez-Salinero, J. Sheu, and Y. Mok, 1988, In situ seismic testing of hard-to-sample soils by surface wave method, in J. L. Von Thus, ed., arthquake engineering and soil dynamic II — Recent advances in ground-motion evaluation: American Society of Civil Engineers, 264–277.

Xia, J., R. D. Miller, and C. B. Park, 1999, Estimation of near-surface shear-wave velocity by inversion of Rayleigh waves: Geophysics, 64, 691–700.

Xia, J., Miller, R. D., Park, C. B., Wightman, E., and Nigbor, R., 2002a, A pitfall in shallow shear-wave refraction surveying: Journal of Applied Geophysics **51**, 1 – 9.

Xia, J., Miller, R.D., Park, C.B., Hunter, J. A., Harris, J. B., and Ivanov, J., 2002b, Comparing shear wave velocity inverted from multichannel surface wave with bore hole measurements: Solid Dynamics and Earthquake Engineering, **22**, 181-190.

Zeidouni, M., 2011, Analytical and inverse models for leakage CO2 storage: Ph.D. dissertation, University of Calgary.

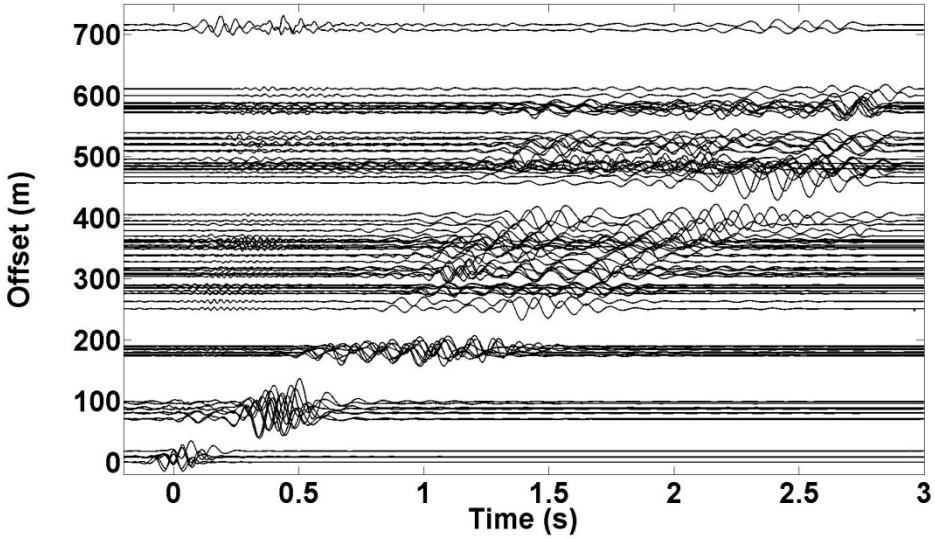

Fig. 1. Traces in a bin.

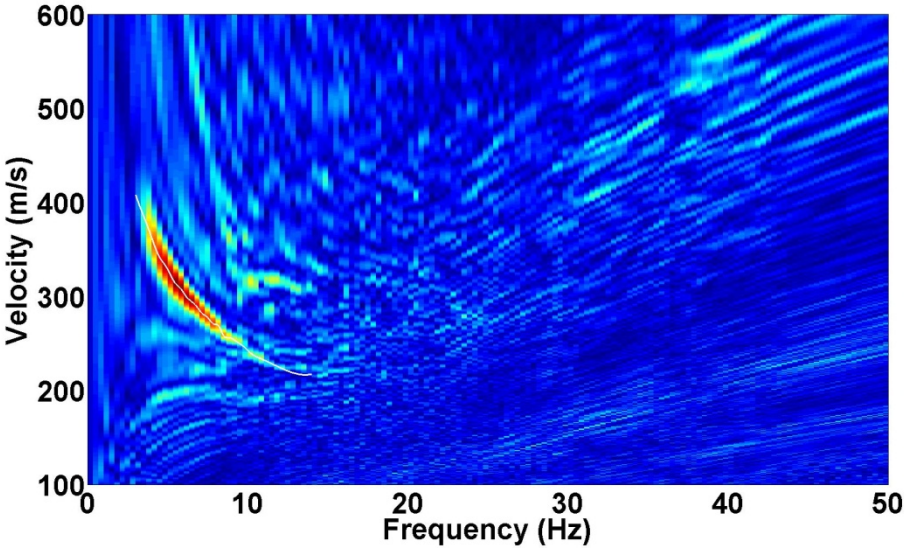

Fig. 2. The phase velocity of the bin in 2.

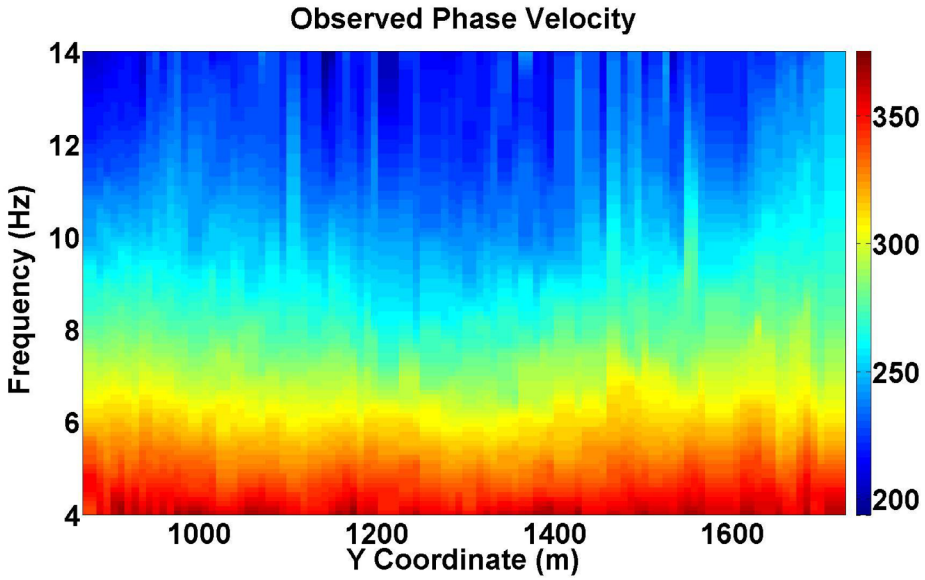

Fig. 3. The observed phase velocity for all the bins in the first data set.

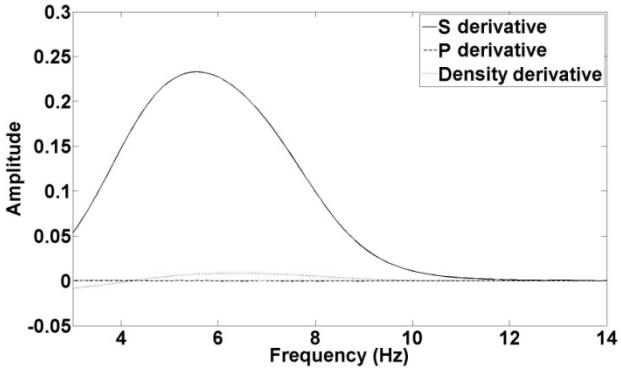

Fig. 4. Phase velocity derivative with respect to S, P velocities and density respectively for the fifth layer.

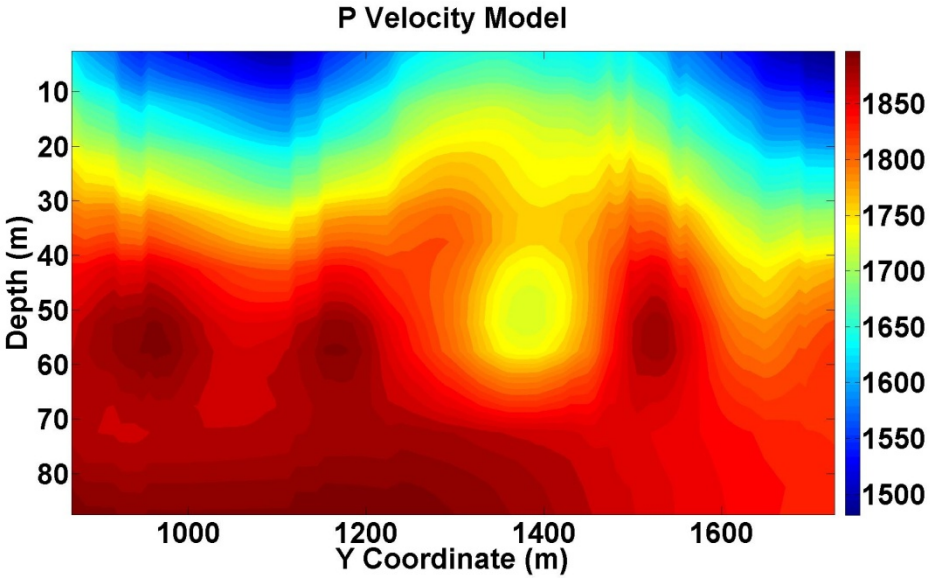

Fig. 5. The P velocity model used for the first data set.

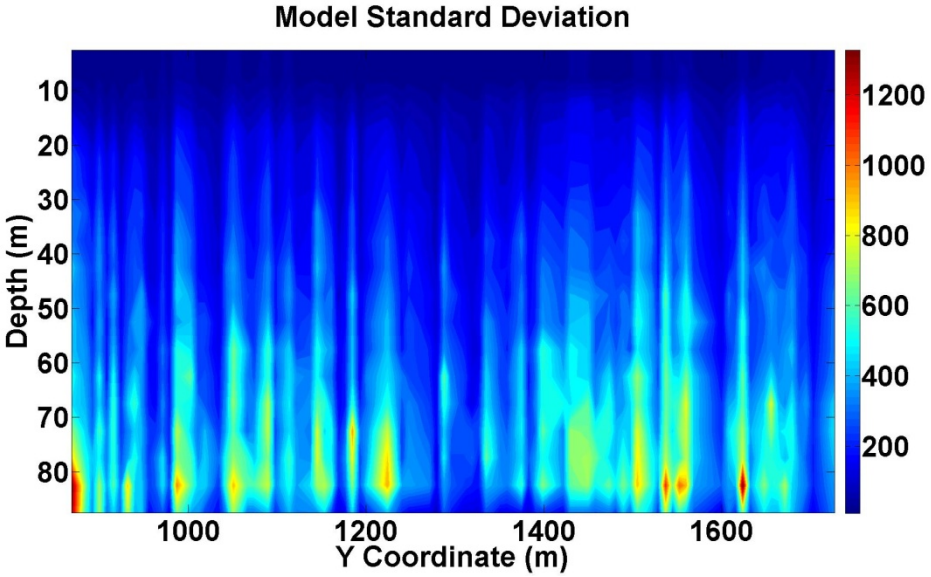

Fig. 6. The standard deviation of the model parameters.

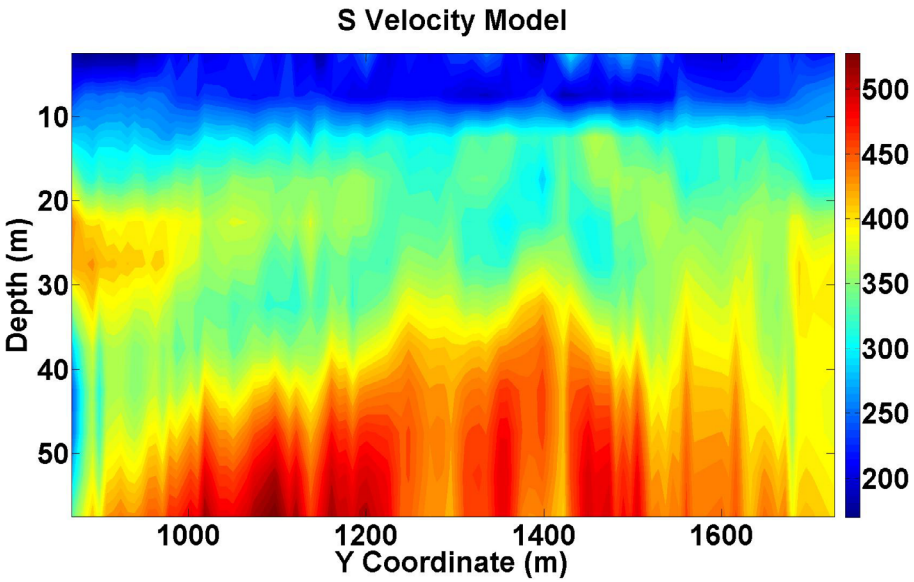

Fig. 7. Obtained S velocity model for the first data set.

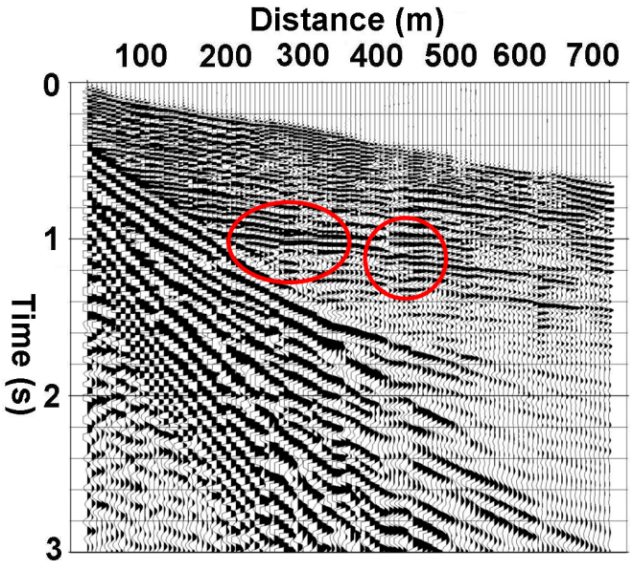

Fig. 8. A shot record without correction.

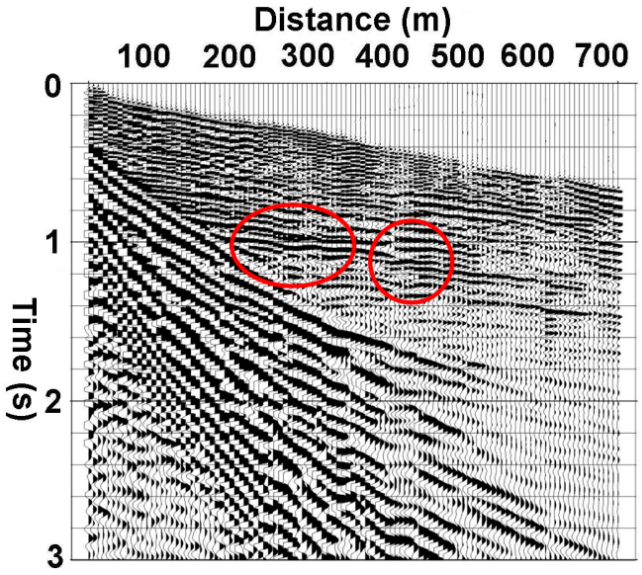

Fig 9: CCSW static corrected.

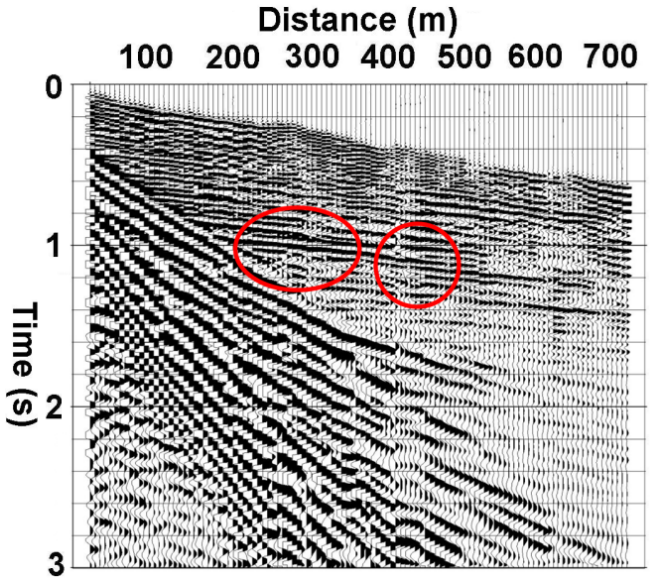

Fig. 10. Non-physical Horizon based trim static corrected.

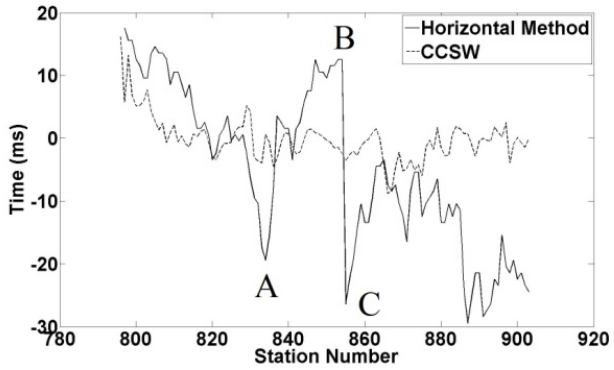

Fig. 11. Static corrections obtained from the non-physical horizon based trim static and CCSW methods respectively.

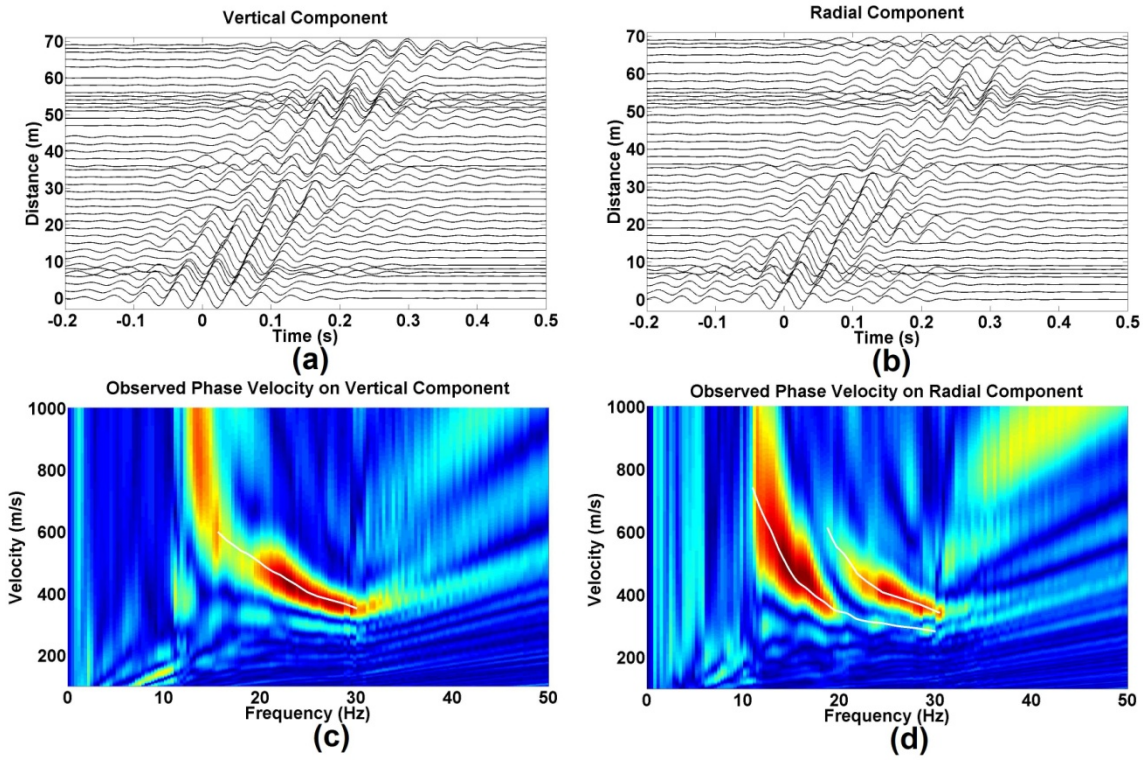

Fig. 12. (a) and (b) Vertical and radial components of a bin in the Priddis data respectively, (c) observed phase velocity in (a) and (d) observed phase velocity in (d).

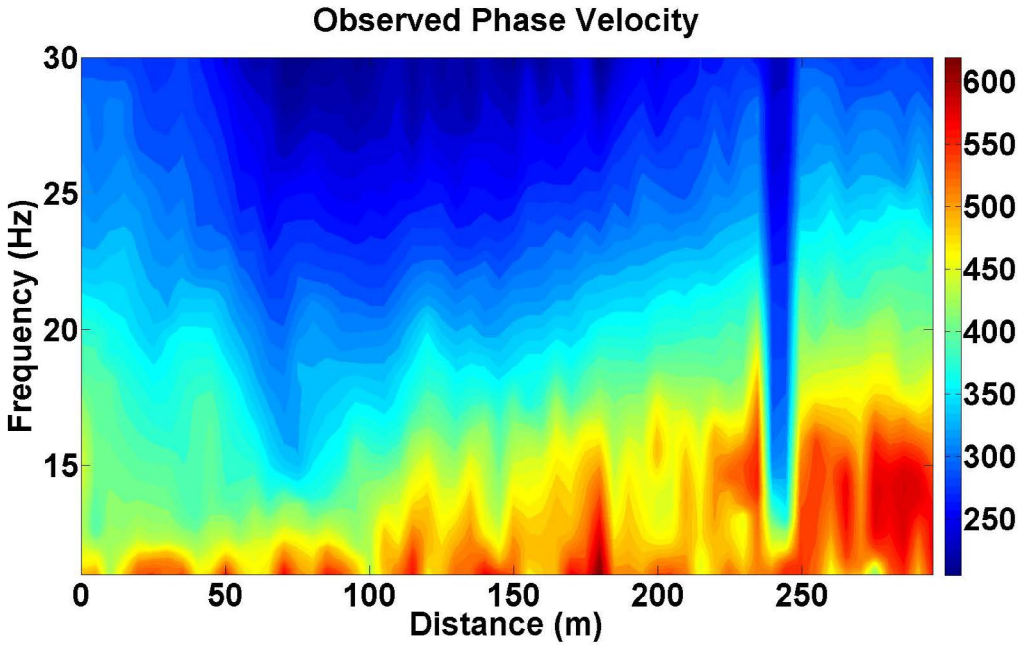

Fig. 13. The observed phase velocity for all the bins for the Priddis data.

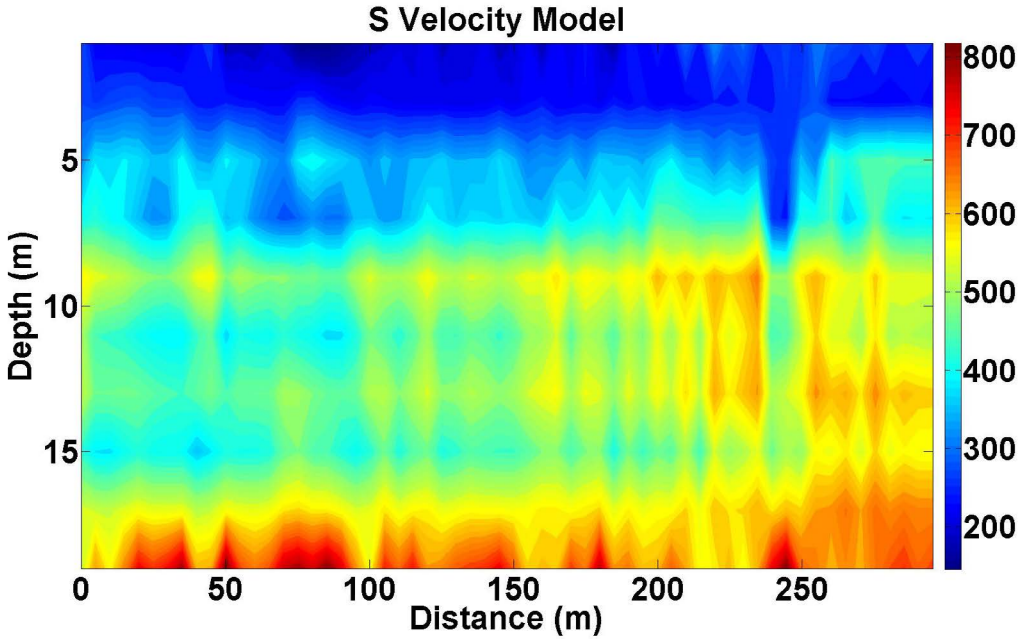

Fig. 14. S velocity Model for the Priddis data.

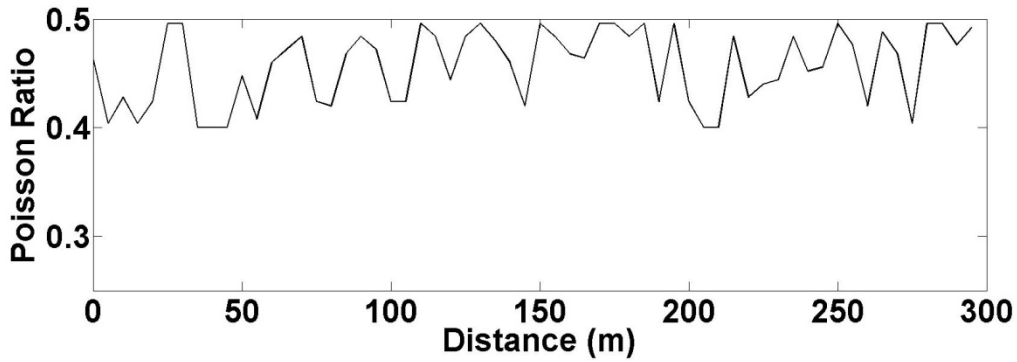

Fig. 15. Obtained Poisson ratios.

S Velocity	P velocity	Density
241	1654	2000
197	1681	2000
333	1721	2000
343	1742	2000
321	1760	2000
329	1772	2000
370	1790	2000
415	1793	2000
444	1777	2000
459	1766	2000

Table 1: The geological model used for the calculation of the derivatives in Figure 4. The thickness for each layer is 5m.